Research Article

Redirection of the glycolytic flux enhances isoprenoid production in *Saccharomyces cerevisiae*

Suryang Kwak[1,2]

Eun Ju Yun[2,3]

Stephan Lane[1,2]

Eun Joong Oh[1,2]

Kyoung Heon Kim[3]

Yong-Su Jin[1,2]

[1]Department of Food Science and Human Nutrition, University of Illinois at Urbana-Champaign, Urbana, IL, USA

[2]Carl R. Woese Institute for Genomic Biology, University of Illinois at Urbana-Champaign, Urbana, IL, USA

[3]Department of Biotechnology, Korea University, Seoul, Republic of Korea

Correspondence: Dr. Yong-Su Jin, Department of Food Science and Human Nutrition, University of Illinois at Urbana-Champaign, 1206 West Gregory Dr., IGB1105, Urbana, Illinois, 61801, USA.

E-mail: ysjin@illinois.edu

Keywords: Isoprenoid, *Saccharomyces cerevisiae*, NADPH, Oxidative pentose phosphate pathway, Phosphofructokinase

Abbreviations: MVA, mevalonate; **HMG-CoA,** 3-hydroxy-3-methyl-glutaryl-coenzyme A; **HMGR,** HMG-CoA reductase; **G6P,** glucose-6-phosphate; **F6P,** fructose-6-phosphate; **G6PD,** glucose-6-phosphate dehydrogenase; **PP,** pentose phosphate; **PFK,** phosphofructokinase; **Asp**, aspartic acid; **Ser**, serine; **gRNA,** guide RNA; **dDNA,** donor DNA; **HCA,** hierarchical cluster analysis; **PCA,** principal component analysis; **GPD,** glycerol-3-phosphate dehydrogenase; **GPP,** glycerol phosphatase; **P_i,** inorganic phosphate; **DHAP**, dihydroxyacetone phosphate; **ADS,** amorphadiene synthase; **GA3PD,** glyceraldehyde-3-phosphate dehydrogenase

Abstract

Sufficient supply of NADPH is a prerequisite of the overproduction of isoprenoids and related bioproducts in *Saccharomyces cerevisiae.* Although *S. cerevisiae* highly depends on the oxidative pentose phosphate (PP) pathway to produce NADPH, its metabolic flux toward the oxidative PP pathway is limited due to the rigid glycolysis flux. To maximize NADPH supply for the isoprenoid production in yeast, upper glycolytic metabolic fluxes were reduced by introducing mutations into phosphofructokinase (PFK) along with overexpression of *ZWF1* encoding glucose-6-phosphate (G6P) dehydrogenase. The PFK mutations (Pfk1 S724D and Pfk2 S718D) resulted in less glycerol production and more accumulation of G6P which is a gateway metabolite toward the oxidative PP pathway. When combined with the PFK mutations, overexpression of *ZWF1* caused substantial increases of [NADPH]/[$NADP^+$] ratios whereas the effect of *ZWF1* overexpression alone in the wild-type strain was not noticeable. Also, the introduction of *ZWF1* overexpression and the PFK mutations into engineered yeast overexpressing acetyl-CoA C-acetyltransferase (*ERG10*), truncated HMG-CoA reductase isozyme 1 (*tHMG1*), and amorphadiene synthase (*ADS*) led to a titer of 497 mg/L of amorphadiene (3.7-fold over the parental strain). These results suggest that perturbation of upper glycolytic fluxes, in addition to *ZWF1* overexpression, is necessary for efficient NADPH supply through the oxidative PP pathway and enhanced production of isoprenoids by engineered *S. cerevisiae*.

1. Introduction

Isoprenoids constitute the largest and structurally most diverse class of natural organic compounds [1]. Isoprenoids have been widely used in pharmaceutical, cosmetic, food, and biofuel industries due to their various biological functions and high energy densities [1-4]. Despite their essential roles in living organisms, however, the levels of isoprenoids in native sources are generally insufficient to achieve commercial production [1]. Thus, various metabolic engineering approaches have been undertaken to overcome the limited isoprenoid contents of microorganisms.

Saccharomyces cerevisiae is a representative microbial host that has been engineered to produce diverse isoprenoid molecules [5–9]. *S. cerevisiae* synthesizes C5 monomers of isoprenoids, namely isopentenyl diphosphate and dimethylallyl diphosphate, through the mevalonate (MVA) pathway [10,11]. Hence, previous studies of the isoprenoid overproduction by *S. cerevisiae* have mainly focused on metabolic engineering of the MVA pathway [6,12–15]. Especially, 3-hydroxy-3-methyl-glutaryl-coenzyme A (HMG-CoA) reductase (HMGR), a rate-limiting enzyme of the MVA pathway, has been a major engineering target. Truncation of the regulatory domain of HMGR was considered as the most influential genetic alternation for enhanced isoprenoid production in *S. cerevisiae* [16]. Cofactor engineering for HMGR, which originally requires 2 NADPH per reaction, was another successful approach. For instance, the production of C15 isoprenoids (sesquiterpenes) α-santalene, and farnesene improved by increasing cellular NADPH availability [9], and altering cofactor preference of HMGR to NADH [17], respectively.

The intracellular ratios of NADPH/$NADP^+$ and NADH/NAD^+ play key roles in more than 200 metabolic reactions of *S. cerevisiae* including HMGR [18]. *S. cerevisiae*

has three major NADPH sources—(i) glucose-6-phosphate dehydrogenase (G6PD, *ZWF1*) that catalyzes the first reaction of oxidative pentose phosphate (PP) pathway, (ii) $NADP^+$-dependent aldehyde dehydrogenase (*ALD6*), and (iii) $NADP^+$-specific isocitrate dehydrogenase (*IDP2*) [19]. During utilization of fermentable sugars including glucose, NADPH production by *S. cerevisiae* highly depends on the oxidative PP pathway [19]. Therefore, theoretically, the increase of glucose-6-phosphate (G6P) fluxes toward the oxidative PP pathway through G6PD instead of glycolysis can effectively improve NADPH production further (Fig. 1B). However, *S. cerevisiae* exhibits limited G6P fluxes toward the oxidative PP pathway during glucose utilization due to its rigid metabolic flux through glycolysis [20–22]. Allosteric activation of phosphofructokinase (PFK) by fructose-2,6-bisphosphate is the mainspring of the rigid metabolism of upper glycolysis in *S. cerevisiae* [23]. As such, deletion of the fructose-2,6-bisphosphate synthetic pathway causes accumulation of intermediates of upper glycolysis, such as G6P and fructose-6-phosphate (F6P) [24].

In this study, we engineered PFK as well as G6PD to increase G6P fluxes through the oxidative PP pathway in *S. cerevisiae* (Fig. 1A) and investigated metabolic changes including the enhanced NADPH level caused by the two metabolic perturbations. Specifically, *ZWF1* encoding G6PD was overexpressed. Simultaneously, to maximize G6P supply for G6PD, the allosteric activation mechanism of PFK was disrupted by mutating amino acid residues which are involved in the interaction between fructose-2,6-bisphosphate to PFK isozymes. As a result, *ZWF1* overexpression and mutation of PFK synergistically increased the [NADPH]/[$NADP^+$] ratio, while *ZWF1* overexpression did not lead to significant changes on NADPH levels in the strains

possessing wild-type PFK, and the resulting engineered strains exhibited enhanced production of amorphadiene accordingly. This study illustrates how inactive upper glycolysis affects NADPH availability in glucose-grown *S. cerevisiae* and expands the range of metabolic engineering strategies to enhance the production of diverse biofuels and bioproducts whose biosynthetic pathways are NADPH-dependent.

2. Materials and methods

2.1. Plasmids and donor DNAs

The plasmids, primers, and guide RNAs (gRNAs) sequences used in this study were summarized in Table S1, Table S2, and Table S3. Polymerase chain reaction (PCR) was performed using Q5® High-Fidelity DNA Polymerase (New England Biolabs, Ipswich, MA, USA) unless otherwise stated. gRNAs with the target sequences near the 2172nd base pair of *PFK1* and the 2154th base pair of *PFK2* (Fig. 2A) were bracketed by ere inserted into 2-micron plasmids carrying antibiotic-resistance markers, and resulting plasmids were named pRS42K-P1M and pRS42H-P2M, respectively (Table S1). Plasmids of gRNAs targeting promoter regions of *ZWF1* and *ERG9* were prepared through ligation-independent FastCloning [25] from pRS42K-P1M and pRS42H-P2M, respectively. Plasmids for constitutive expression of *ERG10*, *tHMG1*, and *ADS* were constructed based on 2-micron plasmids carrying auxotrophic markers (Table S1).

To prepare double-stranded donor DNAs (dDNAs) for CRISPR-Cas9 genome editing, Phusion® High-Fidelity PCR Master Mix with HF buffer (New England Biolabs) and relevant dDNA primer sets were employed. Two dDNAs overlapping point mutation sites of *PFK1* and *PFK2* were prepared using primer sets of dD-mPFK1 and dD-mPFK2

by overlap extension PCR. dDNAs containing promoter region of *CCW12* (P_{CCW12}) and *SYH1* (P_{SYH1}) were PCR amplified from genomic DNA of D452-2 strain using primer sets of dD-PZC and dD-PES, respectively. dDNA PCR products were subsequently concentrated and purified through ethanol acetate precipitation.

2.2. Media and culture conditions

Yeast peptone medium (10 g/L yeast extract, 20 g/L peptone) containing 20 g/L of glucose (YPD) was prepared for yeast genome editing and enzyme assays. Nourseothricin (100 μg/mL), geneticin (300 μg/mL), and hygromycin B (200 μg/mL) were added to YPD medium if required for selection. Synthetic complete (SC) medium, which contains yeast nitrogen base and complete supplement mixture without histidine, leucine, and uracil (MP Biomedicals, Santa Ana, CA, United States), was used to select and culture transformants of plasmids containing an auxotrophic marker. 20 g/L of glucose and agar were added to prepare selection plates. To analyze metabolites of engineered yeasts, or produce amorphadiene, aerobic cultures were performed in 50 mL SC medium containing 40 g/L of glucose and 50 mM potassium hydrogen phthalate buffer (pH 5.5) in a 250 mL baffled flask shaken at 250 rpm. To trap volatile products including amorphadiene, 5 mL dodecane was added after filter sterilization using Millex®-MP 0.22μm filter unit (EMD Millipore, Billerica, MA, USA). *Escherichia coli* Top10 strain was used for routine plasmid cloning. *E. coli* strains were aerobically grown in Luria Bertani medium (5 g/L yeast extract, 10 g/L tryptone, and 5 g/L NaCl), at 37˚C, and 100 μg/mL of ampicillin was supplemented if required. Cell growth was

monitored by absorbance at 600 nm (A_{600}) using BioMate 5 UV-visible spectrophotometer (Thermo Fisher Scientific, Waltham, MA, USA).

2.3. Yeast genetic engineering

Genotypes of yeast strains used in this study are summarized in Table 1. *S. cerevisiae* D452-2 strain [26] was a parental strain. Plasmids and dDNAs were introduced to yeasts by lithium acetate/single strand carrier DNA/polyethylene glycol method [27]. PFK mutagenesis and promoter substitutions were performed using CRISPR-Cas9 genome editing [28]. To construct the PFK mutant strain, two gRNA-expressing plasmids (pRS42K-P1M and pRS42H-P2M) and two dDNAs (dDNA-mPFK1 and dDNA-mPFK2) were simultaneously transformed into the D452-2 strain carrying Cas9-NAT plasmid (Addgene #64329) (Fig. 2A and S1A). P_{CCW12} was inserted between the open reading frame and corresponding original promoter region of *ZWF1* by introducing pRS42K-PZ and dDNA-PZC into yeast strains carrying Cas9-NAT. *ERG9* promoter was substituted by P_{SYH1} through an identical process but using pRS42H-PE and dDNA-PES (Fig. S1B). Correct transformants were selected from YPD plates containing proper antibiotics, then confirmed by colony PCR and sequencing. Transformants of 2-micron auxotrophic plasmids or their derivatives expressing core enzymes for the amorphadiene production (Table S1) were selected from SCD plates without histidine, leucine, and uracil.

2.4. Glucose-6-phosphate dehydrogenase assay

Crude cell lysates were prepared in the middle of the exponential growth [29]. The enzyme reaction was initiated by adding 1 μL of crude cell lysate in a reaction mixture consisting of 171 μL of 100 mM pH 7.6 triethanolamine buffer, 14 μL of 100 mM $MgCl_2$, 7 μL of 10 g/L G6P, and 7 μL of 10 g/L NADP sodium salt hydrate. Assays were conducted by Synergy 2 microplate reader (Biotek, Winooski, VT, USA) with 96-well plate at 30˚C. The increase of NADPH concentration was measured at 340 nm and the NADPH molar extinction coefficient 6.22 $mM^{-1}cm^{-1}$ was used for calculation. One G6PD activity unit was defined as the amount of enzyme catalyzing the reduction of 1 μmol of NADP per minute. Activities were normalized by protein concentration of reaction mixtures. Protein concentrations were measured using Pierce™ BCA Protein Assay Kit (Thermo Fisher Scientific).

2.5. Analysis of intracellular metabolites and redox cofactors

Flux balance analysis (FBA, Fig. 1B) was performed using the COBRApy package [30] and the iMM904 yeast metabolic model [31]. The total sum of all NADPH-producing reactions was monitored as the flux was pushed through the G6PD reaction towards the oxidative PP pathway.

10^7 cells of engineered strains were harvested at both middles of glucose consuming phase and ethanol consuming phase. Intracellular metabolites were extracted by the fast filtration method [32] with small modifications. Cells were vacuum-filtered through nylon membrane filters (0.45 μm pore size, 13 mm diameter; Whatman, Maidstone, United Kingdom) and washed by filtrating 2 mL of distilled water within 30

sec. Filters and washed cells were quickly mixed with 1 mL of acetonitrile/water mixture (1:1, v/v) and 0.1 g of glass beads in 1.5 mL tubes, and the mixtures were vigorously vortexed for 5 min. The mixtures were then centrifuged at 13,000 rpm and 4˚C for 10 min. 500 µL of supernatants were collected and vacuum-dried. Dried samples were chemically derivatized by sequential treatments of 40 mg/mL methoxyamine hydrochloride in pyridine and 45 µL of N-methyl-N-trimethylsilyl trifluoroacetamide. Derivatized samples were analyzed by gas chromatography-mass spectrometry (GC-MS, 7890A GC/5975C MSD system; Agilent Technology, Wilmington, DE, United States) equipped with an HP-5MS column (30 m × 0.25 µm, 0.25 µm; Agilent Technology). The thermal program was as follows; the initial temperature of 80°C for 1 min, and then ramping to 300°C at 10°C/min with a holding time of 1 min at 300°C. Helium constantly flowed at 1 mL/min as a carrier gas. Mass spectra were acquired in a scan range from 85 to 700 m/z and an electron impact was 70 eV. The temperature of the inlet and MS transfer line were 250˚C. Raw metabolome data were processed using AMDIS [33], SpectConnect [34], and Golm Metabolome Database [35]. To measure cellular concentrations of redox cofactor NADPH and $NADP^+$, cells were harvested by centrifugation at 13,000 rpm and 4˚C for 10 min. Cell pellets were washed using ice cold distilled water. NADPH and $NADP^+$ were extracted from yeast cells and determined by EnzyChrom™ $NADP^+$/NADPH Assay Kit (BioAssay Systems, Hayward, CA, USA) and Synergy 2 microplate reader (Biotek). Statistical analyses were performed in R using the pheatmap, ggplot2, and ggbiplot packages.

2.7. Analysis of extracellular metabolites and amorphadiene

Glucose, glycerol, acetate, and ethanol concentrations were determined by Agilent 1200 high-performance liquid chromatography (HPLC) system equipped with a refractive index detector (Agilent Technologies). 0.005 N H_2SO_4 was eluted through Rezex ROA-Organic Acid H^+ (8%) column (Phenomenex, Torrance, CA, USA) at 0.6 mL/min and 50˚C. Amorphadiene in dodecane layer was quantified by GC-MS (7890A GC/5975C MSD system; Agilent Technology) and RTX-5Sil MS column (30 m × 0.25 mm, 0.25 μm; Restek, Bellefonte, PA, USA). Helium constantly flowed at 1 mL/min as a carrier gas. The temperature of the inlet and MS transfer line were 250°C. The initial oven temperature was 150°C for 0.75 min followed by a ramp of 40°C/min to a final temperature of 250°C for 3 min. 20 μL of dodecane layer was separated from cultures and mixed with 980 μL of ethyl acetate which was spiked by 15 mg/L of trans-caryophyllene. 1 μL of samples and trans-caryophyllene standards were injected splitlessly. The caryophyllene and the amorphadiene peaks appeared at 3.73 and 3.89 min, respectively. Amorphadiene concentration was calculated using on the trans-caryophyllene standard curve [36].

3. Results

3.1. Construction and phenotypic characterization of engineered yeast strains

Mutagenesis substituting aspartic acid (Asp) for serine (Ser) residues, which are involved in the binding of fructose-2,6-bisphosphate to PFK isozymes (Pfk1 Ser724Asp and Pfk2 Ser718Asp) [23], was accomplished through CRISPR-Cas9 genome editing (Fig. 2A and S1A). The resulting mutant strain was named SK1. A strong constitutive

promoter P_{CCW12} [37,38] was introduced into an upstream region of *ZWF1* open reading frame to enhance G6PD expression levels in the D452-2 and SK1 strains (Fig. S1B), and the resulting strains were named DZ and SZ, respectively (Table 1). Empty plasmids pRS423, pRS425, and pRS426 were introduced into the strains (D452-2, SK1, DZ, and SZ) to compare phenotypes and metabolomic patterns of parental and engineered strains without a heterologous isoprenoid synthetic pathway. Substitution of the endogenous promoter of *ZWF1* (P_{ZWF1}) with a strong promoter (P_{CCW12}) increased cellular G6PD activities in engineered strains (Fig. 2B and S2). The increased G6PD activities resulted in reduced production of acetate by the DZ and SZ strains (Fig. 2C and S3C) which is coupled with NADPH production in yeast, indicating the *ZWF1*-overexpressing strains might have altered intracellular levels of NADPH. The strains possessing mutant PFK (SK1 and SZ) exhibited drastic decreases in glycerol yields as compared to corresponding parental strains (D452-2 and DZ), while they did not exhibit noticeable changes in ethanol yields (Fig. 2C and S3).

To reduce metabolic fluxes from farnesyl pyrophosphate toward ergosterol biosynthesis, a weak promoter P_{SYH1}, which exhibited identical transcription levels on both fermentable and non-fermentable carbon sources [39], was integrated at the upstream region of *ERG9* in the D452-2, DZ, SK1, and SZ strains, and resulting strains were named the De, DZe, Se, and Sze strains, respectively (Table 1). Down-regulation of *ERG9* expression under the control of P_{SYH1} did not lead to significant changes in yields of biomass and metabolic products during glucose fermentation (Fig 2D and S3). Less glycerol production was still the most obvious phenotypic change of the SK1 derivative strains (Se and SZe) (Fig. S3b).

3.2. Increased availabilities of upper glycolysis intermediates in the PFK mutant

We next investigated the levels of intracellular metabolites in the De, DZe, Se, and SZe strains to closely assess the outcome of *ZWF1* overexpression and the PFK mutations on the central carbon metabolism of the engineered yeasts. As ethanol, the major product of glucose fermentation of *S. cerevisiae*, has been characterized as a decent carbon source to produce isoprenoids by engineered yeast [7,40], glucose cultures were continued until the control strain (De) re-assimilated the produced ethanol, and samples for intracellular metabolite analyses were collected at 20 h and 136 h, in the middle of glucose and ethanol utilization phases, respectively (Fig. 3A). The identified metabolites were subjected to hierarchical cluster analysis (HCA) and principal component analysis (PCA) to identify differences among the intracellular metabolite profiles of the four engineered strains (De, DZe, Se, and Sze). Both HCA and PCA showed clear metabolomic separations by the PFK mutations and *ZWF1* overexpression during glucose utilization (Fig. 3B and S5A). The PFK mutant strains (Se and Sze) exhibited higher abundances of upper glycolysis intermediates G6P and F6P in comparison with the De and DZe strains (Fig. 3B). During ethanol utilization, however, these perturbations did not lead to sharp metabolomic divergences including abundances of G6P and F6P (Fig. S4 and S5B).

3.3. Changes in glycerol metabolic pattern by the PFK mutations

S. cerevisiae oxidizes NADH and produces inorganic phosphate (P_i) by converting dihydroxyacetone phosphate (DHAP) into glycerol through two enzymatic steps of

glycerol-3-phosphate dehydrogenase (GPD) and glycerol phosphatase (GPP) (Fig. 3C). During the glucose consumption phase, intracellular glycerol levels were also lower in the Se and Sze strains with the PFK mutations than the De and DZe strains with the wild-type PFK (Fig. 3B), similar with their extracellular glycerol production profiles (Fig. 2D and S3B). Intriguingly, the Se and SZe strains with the PFK mutations showed higher abundances of glycerol-3-phosphate, an intermediate of the glycerol production pathway (Fig. 3C) as compared to the De and DZe strains (Fig. 3B). As surplus NADH and lower P_i levels—caused by rapid upper glycolysis phosphorylation—drive GPD and GPP reactions [41–43] (Fig. 3C), high glycerol-3-phosphate and low glycerol levels of SK1 derivative strains indicate that the PFK mutations did not perturb the native NADH/NAD^+ balance rather led to more balanced P_i homeostasis in *S. cerevisiae*. Indeed, intracellular P_i levels of the Se and SZe strains were higher than those of De and DZe strains (Fig. 3B).

3.4. Effect of the PFK mutations and *ZWF1* overexpression on NADPH availability

Despite enhanced G6P availabilities (Fig. 3B) and G6PD activities (Fig. 2B) in the SZe strain, PP pathway metabolites could not be detected from the SZe strain as well as other engineered strains under our culture and analysis conditions (Fig. 3B). Instead, higher levels of C5 sugar alcohols derived from the PP pathway such as arabitol and ribitol [44,45] were observed in the DZe and SZe strains that overexpress *ZWF1* (Fig. 3B).

To directly assess the effect of *ZWF1* overexpression and the PFK mutations on the NADPH availability, we evaluated the ratio of NADPH and $NADP^+$ levels of

engineered yeast strains. Concentrations of NADPH and $NADP^+$ were measured from the engineered yeast cells which were collected in the middle of both glucose and ethanol utilization phases to determine NADPH availabilities on the two carbon sources. During the glucose utilization, the combination of *ZWF1* overexpression and the PFK mutations in the SZe strain notably increased the [NADPH]/[$NADP^+$] ratio. Individual perturbations (DZe and Se) also increased the [NADPH]/[$NADP^+$] ratio, but the impacts were not statistically significant (Fig. 3D). The [NADPH]/[$NADP^+$] ratio of the SZe strain was 75%, 46%, and 40% higher as compared to De, DZe, and Se strains, respectively. However, the engineered strains did not show significant differences in the [NADPH]/[$NADP^+$] ratio during ethanol utilization (Fig. 3D).

3.5. Synergistic effects of the PFK mutations and *ZWF1* overexpression on the amorphadiene production

The advantage of the PFK mutations and *ZWF1* overexpression for the production of an isoprenoid was assessed via the production of amorphadiene, a prospective sesquiterpene in the bioenergy and pharmaceutical industries [12,46], as a model isoprenoid. Overexpression plasmids for core elements of amorphadiene biosynthesis [37], namely acetyl-CoA C-acetyltransferase (*ERG10*), truncated HMGR isozyme 1 (*tHMG1*), and amorphadiene synthase (*ADS*), substituted empty plasmids in the De, DZe, Se, and SZe strains. The resulting strains were named De-EHA, DZe-EHA, Se-EHA, and SZe-EHA, respectively (Table 1). Aerobic cultures of the engineered strains were initiated with 45 g/L of glucose and completed when the control strain De-EHA

sequentially depleted glucose and ethanol to allow the engineered strains to synthesize amorphadiene from both carbon sources (Fig. 4A).

During the glucose utilization period (0 h – 38 h), the amorphadiene yield improved 2-fold by *ZWF1* overexpression (DZe-EHA) and 2.4-fold by the PFK mutations (Se-EHA) as compared to the control strain (De-EHA). The combination of *ZWF1* overexpression and the PFK mutations (SZe-EHA) led to the highest amorphadiene yield, which was 3.7-fold higher than the control strain (Fig. 4B).

During the ethanol-utilizing phase (88 h – 234 h), the amorphadiene yield improved noticeably by *ZWF1* overexpression (DZe-EHA and Sze-EHA) (Fig. 4B). However, the amorphadiene yield was not remarkably affected by the PFK mutations. As a result, after sequential utilization of glucose and ethanol (234 h), the SZe-EHA strain achieved the highest amorphadiene titer (497 mg/L), which was 3.94-, 1.68-, and 1.87-fold higher than that of the De-EHA (126 mg/L), DZe-EHA (295 mg/L), and Se-EHA (266 mg/L) strains, respectively (Fig. 4A).

4. Discussion

To improve the isoprenoid biosynthetic capability of *S. cerevisiae*, we aimed to increase the availability of NADPH by manipulating metabolic fluxes through the oxidative PP pathway. We hypothesized that the strong and rigid upper glycolysis of *S. cerevisiae* during glucose utilization [20–22] decreases the availability of G6P for G6PD, accordingly limits metabolic fluxes through the oxidative PP pathway. Indeed, overexpression of *ZWF1* enhanced G6PD activities (Fig. 2B) but did not lead to impressive changes in the [NADPH]/[$NADP^+$] ratio in *S. cerevisiae* (Fig 3D). It was also

reported that simultaneous upregulation of the PP pathway and downregulation of phosphoglucose isomerase (*PGI1*) in *S. cerevisiae* successfully increased cellular content of fatty acids, whose biosynthesis also demands NADPH [47]. In this study, therefore, we designed two metabolic perturbations to maximize NADPH regeneration; the “pull” of G6P toward the oxidative PP pathway by *ZWF1* overexpression and the “push” on G6P by down-regulating catalytic activities of upper glycolysis via the PFK mutations (Pfk1 S724D and Pfk2 S718D).

Ser^{724} of Pfk1 and Ser^{718} of Pfk2, which are key amino acid residues in binding of the allosteric activator fructose-2,6-bisphosphate to PFK [23], were substituted by an Asp residue to block the allosteric activation of upper glycolysis. The lower glycerol formation, the pattern of intracellular glycerol pathway metabolites, and accumulation of upper glycolysis intermediates after introducing the PFK mutations (Fig. 2C, 2D, and 3B) proved impaired PFK activity in the SK1-derived strains. As active upper glycolysis of *S. cerevisiae* rapidly phosphorylates glucose, and glyceraldehyde-3-phosphate dehydrogenase (GA3PD) uses P_i, operation of upper glycolysis and GA3PD decreases ATP and P_i levels until lower-glycolysis compensates ATP, and GPP of the glycerol pathway regenerate P_i through the glycerol pathway [41,42]. The SK1 derivative strains with the PFK mutations accumulated glycerol-3-phosphate to regenerate NAD^+ but did not efficiently metabolize glycerol-3-phosphate further to regenerate P_i (Fig. 3B), probably due to their relatively inactive upper glycolysis which can cause more balanced P_i homeostasis [42]. Also, increased intracellular G6P and F6P abundances of the SK1 derivative strains were similar to the metabolic distinction of fructose-2,6-bisphosphate-null *S. cerevisiae* [24], indicating restricted metabolic fluxes through PFK.

Higher G6P availability resulting from the PFK mutations enabled a notable increase of the [NADPH]/[$NADP^+$] ratio when combined with overexpression of *ZWF1* in SZe (Fig. 3D). The engineered strains overexpressing core enzymes for amorphadiene biosynthesis also showed evident effects of *ZWF1* overexpression and the PFK mutations on the isoprenoid production during both glucose and ethanol phases (Fig. 4). During glucose phase, the SZe-EHA strain showed a strong synergistic effect of the two metabolic perturbations on the amorphadiene yield, 3.67- and 1.86-fold higher than De-EHA and DZe-EHA, respectively (Fig. 4B). The increase in the amorphadiene yield by *ZWF1* overexpression and PFK mutations was consistent with the trend of the [NADPH]/[$NADP^+$] ratio but more obvious. The gap between increments of amorphadiene yield and the [NADPH]/[$NADP^+$] ratio suggests that the actual NADPH availability for the isoprenoid production could not be fully manifested by the [NADPH]/[$NADP^+$] ratio due to native metabolic reactions involving NADPH [48] and cofactor homeostasis in *S. cerevisiae* [49–51]. Indeed, *ZWF1* overexpression decreased accumulation of acetate whose biosynthesis regenerates NADPH (Fig. S3C). Moreira dos Santos et al. also demonstrated that overexpression of the cytosolic malic enzyme pathway regenerating NADPH decreased PP pathway fluxes but did not noticeably change the [NADPH]/[$NADP^+$] ratio [52].

Interestingly, during glucose utilization, the PFK mutations resulted in higher amorphadiene yield (Fig. 4B, Se-EHA vs. De-EHA) as well as higher [NADPH]/[$NADP^+$] ratio (Fig. 3D, Se vs. De) without *ZWF1* overexpression. We speculate that Ald6—producing NADPH when acetate is produced—might not be involved in this outcome considering similar or lower levels of acetate accumulation by the SK1 and Se strains as

compared to the D452-2 and De strains (Fig. S3C). Also, uneven abundance patterns of α-ketoglutarate-derived amino acids of the Se strains (Fig. 3B, glutamate, glutamine, proline, and arginine) suggest that Idp2—producing NADPH using metabolic fluxes in TCA cycle—might not be involved as well. Rather, the outcome implies that the slowdown of upper glycolytic fluxes by the PFK mutations might increase G6P fluxes toward the oxidative PP pathway even without *ZWF1* overexpression. This phenotype resembles a strategy by which human cancer cells cope with oxidative stress via NADPH-glutathione system; the glycolysis flux of cancer cell can be shunted to the oxidative PP pathway by promoting degradation of PFKFB3 (phosphofructokinase/fructose bisphosphatase type-3) followed by increased metabolic fluxes through the oxidative PP pathway [53].

During ethanol utilization, *ZWF1* overexpression and PFK mutations did not affect the [NADPH]/[$NADP^+$] ratio as notably as during glucose utilization (Fig. 3D). Moreover, the effect of PFK mutations on amorphadiene production from ethanol was insignificant (Fig. 4B). Under ethanol culture conditions, the limited metabolic flux through upper glycolysis [20,54] and the shift of the primary source of NADPH from G6PD to idp2 [19,20] might mitigate the efficacy of *ZWF1* overexpression and PFK mutations on the NADPH availability. Nevertheless, *ZWF1* overexpression increased amorphadiene yield more efficiently during the ethanol phase (Fig. 4B). The distinctive consequence of *ZWF1* overexpression during the ethanol phase implies inefficient biosynthesis of cytosolic acetyl-CoA from glucose, rather than higher NADPH availability on ethanol. The predominantly fermentative metabolism of *S. cerevisiae* converges metabolic fluxes toward ethanol under glucose culture conditions (Fig. S3) by

repressing respiratory metabolic pathways, including acetyl-CoA synthase [55], but a de-repression occurs after glucose depletion [56]. Consequently, the SZe-EHA strain, the combination of *ZWF1* overexpression and the PFK mutations, showed the highest amorphadiene titer and productivity after sequential utilization of glucose and ethanol due to high amorphadiene yields during both glucose and ethanol phases (Fig. 4A).

The current study achieved a new strategy that simultaneously pushes and pulls G6P toward the oxidative PP pathway from glycolysis to effectively enhance NADPH supply for the isoprenoid production in *S. cerevisiae*. Especially, we demonstrated the critical impact of the mutated PFK—cannot interact with its allosteric activator—on NADPH production and isoprenoid production in *S. cerevisiae* using amorphadiene in conjunction with genetic perturbations for the amorphadiene production, such as *ERG9* down-regulation and overexpression of *tHMG1*, *ERG10*, and *ADS*. Despite the minimal metabolic engineering on the MVA pathway, SZe-EHA exhibited higher amorphadiene titer and productivity than previous reports that performed yeast batch cultures with the defined medium and glucose (Table S4). Combinations with further genetic and environmental perturbations including combinatorial engineering of both the MVA pathway [6,7] and the PP pathway [47], optimization of acetyl-CoA biosynthesis [37,47], minimizing ethanol fermentation [37,47], and further manipulation of native metabolisms involving NADPH [9,52] would maximize the positive effect of the shunting glycolysis into the PP pathway on the isoprenoid production. Also, we envision that our strategy of down-regulation of upper glycolysis can be successfully applied for the production of not only isoprenoids but also other biofuels and bioproducts whose biosynthetic pathways are contingent on NADPH or upper glycolysis intermediates.

Acknowledgments

This work was funded by Energy Biosciences Institute and the DOE Center for Advanced Bioenergy and Bioproducts Innovation (U.S. Department of Energy, Office of Science, Office of Biological and Environmental Research under Award Number DE-SC0018420).

Reference

[1] M. C. Y. Chang, J. D. Keasling, Production of isoprenoid pharmaceuticals by engineered microbes. *Nat. Chem. Biol*. **2006**, *2*, 674.

[2] Y. Miura, K. Kondo, T. Saito, H. Shimada, P. D. Fraser, N. Misawa, *Appl. Environ. Microbiol*. **1998**, *64*, 1226.

[3] E. M. Paradise, J. Kirby, R. Chan, J. D. Keasling, *Biotechnol. Bioeng*. **2008**, *100*, 371.

[4] J. D. Keasling, H. Chou, *Nat. Biotechnol*. **2008**, *26*, 298.

[5] J. Yuan, C. B. Ching, *Microb. Cell Factories* **2015**, *14*, 38.

[6] J. Yuan, C. B. Ching, *Biotechnol. Bioeng*. **2014**, *111*, 608.

[7] P. J. Westfall, D. J. Pitera, J. R. Lenihan, D. Eng, F. X. Woolard, R. Regentin, T. Horning, H. Tsuruta, D. J. Melis, A. Owens, S. Fickes, D. Diola, K. R. Benjamin, J. D. Keasling, M. D. Leavell, D. J. McPhee, N. S. Renninger, J. D. Newman, C. J. Paddon, *Proc. Natl. Acad. Sci. U. S. A*. **2012**, *109*, E111.

[8] C. J. Paddon, P. J. Westfall, D. J. Pitera, K. Benjamin, K. Fisher, D. McPhee, M. D. Leavell, A. Tai, A. Main, D. Eng, D. R. Polichuk, K. H. Teoh, D. W. Reed, T. Treynor, J. Lenihan, H. Jiang, M. Fleck, S. Bajad, G. Dang, D. Dengrove, D. Diola, G. Dorin, K. W. Ellens, S. Fickes, J. Galazzo, S. P. Gaucher, T. Geistlinger, R. Henry, M. Hepp, T. Horning, T. Iqbal, L. Kizer, B. Lieu, D. Melis, N. Moss, R. Regentin, S. Secrest, H. Tsuruta, R. Vazquez, L. F. Westblade, L. Xu, M. Yu, Y. Zhang, L. Zhao, J. Lievense, P. S. Covello, J. D. Keasling, K. K. Reiling, N. S. Renninger, J. D. Newman, *Nature* **2013**, *496*, 528.

[9] G. Scalcinati, S. Partow, V. Siewers, M. Schalk, L. Daviet, J. Nielsen, *Microb. Cell Factories* **2012**, *11*, 117.

[10] F. Paltauf, S. D. Kohlwein, S. A. Henry, in *The Molecular and Cellular Biology of the Yeast Saccharomyces*; Cold Spring Harbor Laboratory Press **1992**, *21B*, Ch 8.

[11] S. Kwak, J. H. Jo, E. J. Yun, Y. S. Jin, J. H. Seo, *Biotechnol. Adv*. **2019**, *37*, 271.

[12] D. K. Ro, E. M. Paradise, M. Ouellet, K. J. Fisher, K. L. Newman, J. M. Ndungu, K. A. Ho, R. A. Eachus, T. S. Ham, J. Kirby, M. C. Y. Chang, S. T. Withers, Y. Shiba, R. Sarpong, J. D. Keasling, *Nature* **2006**, *440*, 940.

[13] Z. Dai, Y. Liu, X. Zhang, M. Shi, B. Wang, D. Wang, L. Huang, X. Zhang, *Metab. Eng.* **2013**, *20*, 146.

[14] F. Mantzouridou, M. Z. Tsimidou, *FEMS Yeast Res*. **2010**, *10*, 699.

[15] B. S. J. Davies, H. S. Wang, J. Rine, *Mol. Cell. Biol*. **2005**, *25*, 7375.

[16] K. A. Donald, R. Y. Hampton, I. B. Fritz, *Appl. Environ. Microbiol*. **1997**, *63*, 3341.

[17] A. L. Meadows, K. M. Hawkins, Y. Tsegaye, E. Antipov, Y. Kim, L. Raetz, R. H. Dahl, A. Tai, T. Mahatdejkul-Meadows, L. Xu, L. Zhao, M. S. Dasika, A. Murarka, J. Lenihan, D. Eng, J. S. Leng, C. L. Liu, J. W. Wenger, H. Jiang, L. Chao, P. Westfall, J. Lai, S. Ganesan, P. Jackson, R. Mans, D. Platt, C. D. Reeves, P. R. Saija, G. Wichmann, V. F. Holmes, K. Benjamin, P. W. Hill, T. S. Gardner, A. E. Tsong, *Nature* **2016**, *537*, 694.

[18] X. Chen, S. Li, L. Liu, L, *Trends Biotechnol*. **2014**, *32*, 337.

[19] K. I. Minard, L. McAlister-Henn, *J. Biol. Chem*. **2005**, *280*, 39890.

[20] G. G. Zampar, A. Kümmel, J. Ewald, S. Jol, B. Niebel, P. Picotti, R. Aebersold, U. Sauer, N. Zamboni, M. Heinemann, *Mol. Syst. Biol*. **2013**, *9*, 651.

[21] J. Fiaux, Z. P. Cakar, M. Sonderegger, K. Wüthrich, T. Szyperski, U. Sauer, *Eukaryot. Cell* **2003**, *2*, 170.

[22] A. K. Gombert, M. Moreira dos Santos, B. Christensen, J. Nielsen, *J. Bacteriol.* **2001**, *183*, 1441.

[23] J. J. Heinisch, E. Boles, C. Timpel, *J. Biol. Chem*. **1996**, 271, 15928.

[24] E. Boles, H. W. Göhlmann, F. K. Zimmermann, *Mol. Microbiol*. **1996**, *20*, 65.

[25] C. Li, A. Wen, B. Shen, J. Lu, Y. Huang, Y. Chang, *BMC Biotechnol*. **2011**, *11*, 92.

[26] K. Hosaka, J. Nikawa, T. Kodaki, S. Yamashita, *J. Biochem*. **1992**, *111*, 352.

[27] R. D. Gietz, R. H. Schiestl, *Nat. Protoc*. **2007**, *2*, 31–34.

[28] J. Lian, M. HamediRad, H. Zhao, *Biotechnol. J.* **2018**, *13*, e1700601.

[29] M. Çağlayan, S. Wilson, *Bio-Protoc*. **2014**, *4*, e1312.

[30] A. Ebrahim, J. A. Lerman, B. Ø. Palsson, D. R. Hyduke, *BMC Syst. Biol*. **2013**, *7*, 74.

[31] M. L. Mo, B. Ø. Palsson, M. J. Herrgård, *BMC Syst. Biol*. **2009**, *3*, 37.

[32] S. Kim, D. Y. Lee, G. Wohlgemuth, H. S. Park, O. Fiehn, K. H. Kim, *Anal. Chem.* **2013**, *85*, 2169.

[33] S. E. Stein, J. *Am. Soc. Mass Spectrom*. **1999**, *10*, 770.

[34] M. P. Styczynski, J. F. Moxley, L. V. Tong, J. L. Walther, K. L. Jensen, G. N. Stephanopoulos, *Anal. Chem*. **2007**, *79*, 966.

[35] J. Kopka, N. Schauer, S. Krueger, C. Birkemeyer, B. Usadel, E. Bergmüller, P. Dörmann, W. Weckwerth, Y. Gibon, M. Stitt, L. Willmitzer, A. R. Fernie, D. Steinhauser, *Bioinforma. Oxf. Engl*. **2005**, *21*, 1635.

[36] S. Rodriguez, J. Kirby, C. M. Denby, J. D. Keasling, *Nat. Protoc*. 2014, 9, **1980**.

[37] J. Y. Lee, C. D. Kang, S. H. Lee, Y. K. Park, K. M. Cho, *Biotechnol. Bioeng*. **2015**, *112*, 751.

[38] A. Cankorur-Cetinkaya, E. Dereli, S. Eraslan, E. Karabekmez, D. Dikicioglu, B. Kirdar, *Plos ONE* **2012**, *7*, e38351.

[39] S. Kwak, S. R. Kim, H. Xu, G. C. Zhang, S. Lane, H. Kim, Y. S. Jin, *Biotechnol*. *Bioeng*. **2017**, *114*, 2581.

[40] F. M. Szczebara, C. Chandelier, C. Villeret, A. Masurel, S. Bourot, C. Duport, S. Blanchard, A. Groisillier, E. Testet, P. Costaglioli, G. Cauet, E. Degryse, D. Balbuena, J. Winter, T. Achstetter, R. Spagnoli, D. Pompon, B. Dumas, *Nat. Biotechnol*. **2003**, *21*, 143.

[41] J. H. van Heerden, M. T. Wortel, F. J. Bruggeman, J. J. Heijnen, Y. J. M. Bollen, R. Planqué, J. Hulshof, T. G. O'Toole, S. A. Wahl, B. Teusink, *Science* **2014**, *343*, 1245114.

[42] K. Luyten, J. Albertyn, W. F. Skibbe, B. A. Prior, J. Ramos, J. M. Thevelein, S. Hohmann, *EMBO J.* **1995**, *14*, 1360.

[43] B. M. Bakker, K. M. Overkamp, A. J. A. van Maris, P. Kötter, M. A. H. Luttik, J. P. van Dijken, J. T. Pronk, *FEMS Microbiol*. *Rev*. **2001**, *25*, 15.

[44] M. H. Toivari, H. Maaheimo, M. Penttilä, L. Ruohonen, *Appl. Microbiol. Biotechnol.* **2010**, *85*, 731.

[45] M. E. Lucca, J. F. T. Spencer, L. I. C. de Figueroa, *Appl. Microbiol. Biotechnol*. **2002**, *59*, 472.

[46] P. P. Peralta-Yahya, F. Zhang, S. B. del Cardayre, J. D. Keasling, *Nature* **2012**, *488*, 320.

[47] T. Yu, Y. J. Zhou, M. Huang, Q. Liu, R. Pereira, F. David, J. Nielsen, *Cell* **2018**, *174*, 1549.

[48] J. Nielsen, *J. Bacteriol*. **2003**, *185*, 7031.

[49] J. Förster, I. Famili, P. Fu, B. Ø. Palsson, J. Nielsen, *Genome Res*. **2003**, *13*, 244.

[50] A. Llobell, A. Lopez-Ruiz, J. Peinado, K. Lopez-Barea, *Biochem. J*. **1988**, *249*, 293.

[51] A. Bloem, I. Sanchez, S. Dequin, C. Camarasa, *Appl. Environ. Microbiol*. **2016**, *82*, 174.

[52] M. Moreira dos Santos, V. Raghevendran, P. Kötter, L. Olsson, J. Nielsen, *Metab. Eng.* **2004**, *6*, 352.

[53] T. Yamamoto, N. Takano, K. Ishiwata, M. Ohmura, Y. Nagahata, T. Matsuura, A. Kamata, K. Sakamoto, T. Nakanishi, A. Kubo, T. Hishiki, M. Suematsu, *Nat. Commun*. **2014**, *5*, 3480.

[54] M. Beullens, K. Mbonyi, L. Geerts, D. Gladines, K. Detremerie, A. W. Jans, J. M. Thevelein, *Eur. J. Biochem*. **1988**, *172*, 227.

[55] S. Kratzer, H. J. Schüller, *Mol. Microbiol*. **1997**, *26*, 631.

[56] Y. Chen, V. Siewers, J. Nielsen, *Plos ONE* **2012**, *7*, e42475.

Table 1. Strains used in this study

Name	Description	Reference
D452-2	*S. cerevisiae*, *MATα*, *leu2*, *his3*, *ura3*, and *can1*	[26]
DZ	D452-2, substitution of P_{TDH3} for P_{ZWF1}	This study
SK1	D452-2, mutant *PFK1* (Ser724Asp) and *PFK2* (Ser718Asp)	This study
SZ	SK1, substitution of P_{TDH3} for P_{ZWF1}	This study
De	D452-2, substitution of P_{SYH1} for P_{ERG9}	This study
DZe	DZ, substitution of P_{SYH1} for P_{ERG9}	This study
Se	SK1, substitution of P_{SYH1} for P_{ERG9}	This study
SZe	SZ, substitution of P_{SYH1} for P_{ERG9}	This study
De-EHA	De overexpressing *ERG10*, *tHMG1*, and *ADS* from multicopy plasmids	This study
DZe-EHA	DZe overexpressing *ERG10*, *tHMG1*, and *ADS* from multicopy plasmids	This study
Se-EHA	Se overexpressing *ERG10*, *tHMG1*, and *ADS* from multicopy plasmids	This study
SZe-EHA	SZe overexpressing *ERG10*, *tHMG1*, and *ADS* from multicopy plasmids	This study

Figure captions

Fig. 1. Metabolic engineering approaches in this study. (A) Overview of amorphadiene biosynthesis from glucose in *S. cerevisiae*. The current study up-regulated glucose-6-phosphate dehydrogenase (G6PD) and down-regulated phosphofructokinase (PFK) activities to shunt the glucose-6-phosphate (G6P) flux through glycolysis toward oxidative pentose phosphate (PP) pathway. (B) The theoretical transition of metabolic fluxes on NADPH regeneration (red) and biomass production (gray) by the change in the ratio between G6P fluxes through G6PD (oxidative PP pathway) and phosphofructokinase (glycolysis). F6P, fructose-6-phosphate; F2,6bP, fructose-2,6-bisphosphate; F1,6bP, fructose-1,6-bisphosphate; GA3P, glyceraldehyde-3-phosphate; DHAP, dihydroxyacetone phosphate; IPP, isopentenyl diphosphate; DMAPP, dimethylallyl diphosphate; GPP, geranyl pyrophosphate; FPP, farnesyl pyrophosphate; G6PD, glucose-6-phosphate dehydrogenase; PFK, phosphofructokinase; PPP, pentose phosphate pathway; MVA pathway, mevalonate pathway; Erg10, acetyl-CoA C-acetyl transferase; Erg9, squalene synthase.

Fig. 2. Construction and phenotypic characterization of engineered yeast strains. (A) Mutagenesis of *PFK1* and *PFK2*. Donor DNAs (dDNAs) that have mutations nullifying protospacer adjacent motif (PAM) without amino acid changes, as well as desired mutations (Ser to Asp), recovered double strand breakages resulting from the endonuclease activity of Cas9 guided by corresponding guide RNAs (gRNAs, P1M and P2M). (B) Enhanced glucose-6-phosphate dehydrogenase (G6PD) activities by *ZWF1*

promoter substitution. Activity assays were conducted in quadruplicate independently, and the error bars denote the standard deviation from the means. W, wild-type; M, mutation; O, overexpression; D, down-regulation. (C) Culture profiles of wild-type (D452-2) and engineered strains possessing the mutant PFK (SK1 and SZ) or overexpressing *ZWF1* (DZ and SZ). (D) Culture profiles of wild-type and engineered strains after *ERG9* down-regulation. Symbols and error bars of culture profiles (C and D) denote the mean and the standard deviation of two independent experiments.

Fig. 3. Changes in intracellular metabolites and the [NADPH]/[$NADP^+$] ratio by metabolic perturbations on glycolysis and oxidative pentose phosphate pathway. (A) Glucose and ethanol profiles of the engineered strains (De, DZe, Se, and Sze). Samples for analyses were collected at both middles of the glucose phase (20 h, blue arrow) and ethanol phase (136 h, red arrow). Ethanol phase was indicated in gray. (B) A heat map and hierarchical cluster analysis (HCA) of 53 intracellular metabolites of engineered strains during glucose utilization. Bars highlight glycolysis intermediates (red), glycerol pathway metabolites (gray), C5 sugar alcohols (green), and α-ketoglutarate-derived amino acids (blue). (C) Schematic of consumption and regeneration of energy, redox cofactors, and inorganic phosphate of *S. cerevisiae* grown on glucose. G6P, glucose-6-phosphate; F6P, fructose-6-phosphate; F2,6bP, fructose-2,6-bisphosphate; F1,6bP, fructose-1,6-bisphosphate; GA3P, glyceraldehyde-3-phosphate; DHAP, dihydroxyacetone phosphate; Gly3P, glycerol-3-phosphate; G1,3bP, 1,3-bisphosphoglycerate; P_i, inorganic phosphate; oxPPP, oxidative pentose phosphate pathway; non-oxPPP, non-oxidative pentose phosphate pathway. (D)

[NADPH]/[$NADP^+$] ratios of engineered strains during glucose (20 h) and ethanol utilization (136 h). Data were analyzed by one-way ANOVA followed by Tukey's multiple-comparison test. *, $P < 0.05$; **, $P < 0.01$. All experiments (A, B, and D) were conducted in triplicate, and the error bars denote the standard deviation from the means of independent experiments.

Fig. 4. Amorphadiene production by engineered strains via sequential utilization of glucose and ethanol. (A) Culture profiles of engineered strains expressing the amorphadiene synthetic pathway. The ethanol-consuming phase was indicated in gray. Symbols and error bars of culture profiles denote the mean and the standard deviation of two independent experiments. (B) Effects of carbon sources and metabolic perturbations on the yield of amorphadiene.

Fig. 1.

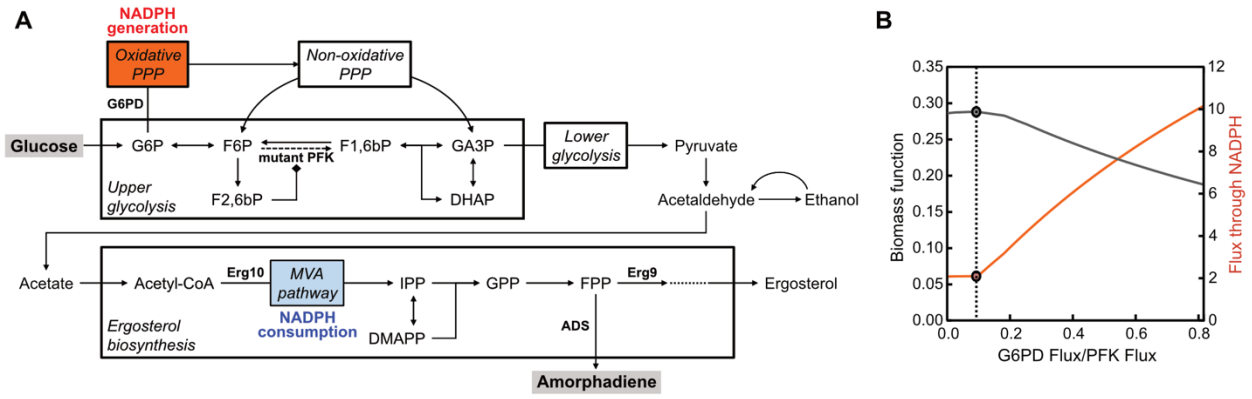
A
NADPH generation
Oxidative PPP
Non-oxidative PPP
G6PD
Glucose
G6P
F6P
mutant PFK
F1,6bP
GA3P
Lower glycolysis
Pyruvate
Upper glycolysis
F2,6bP
DHAP
Acetaldehyde
Ethanol
Acetate
Acetyl-CoA
Erg10
MVA pathway
IPP
GPP
FPP
Erg9
Ergosterol
Ergosterol biosynthesis
NADPH consumption
DMAPP
ADS
Amorphadiene
B
Biomass function
Flux through NADPH
G6PD Flux/PFK Flux
0.35
0.30
0.25
0.20
0.15
0.10
0.05
0.00
12
10
8
6
4
2
0
0.0
0.2
0.4
0.6
0.8

Fig. 2.

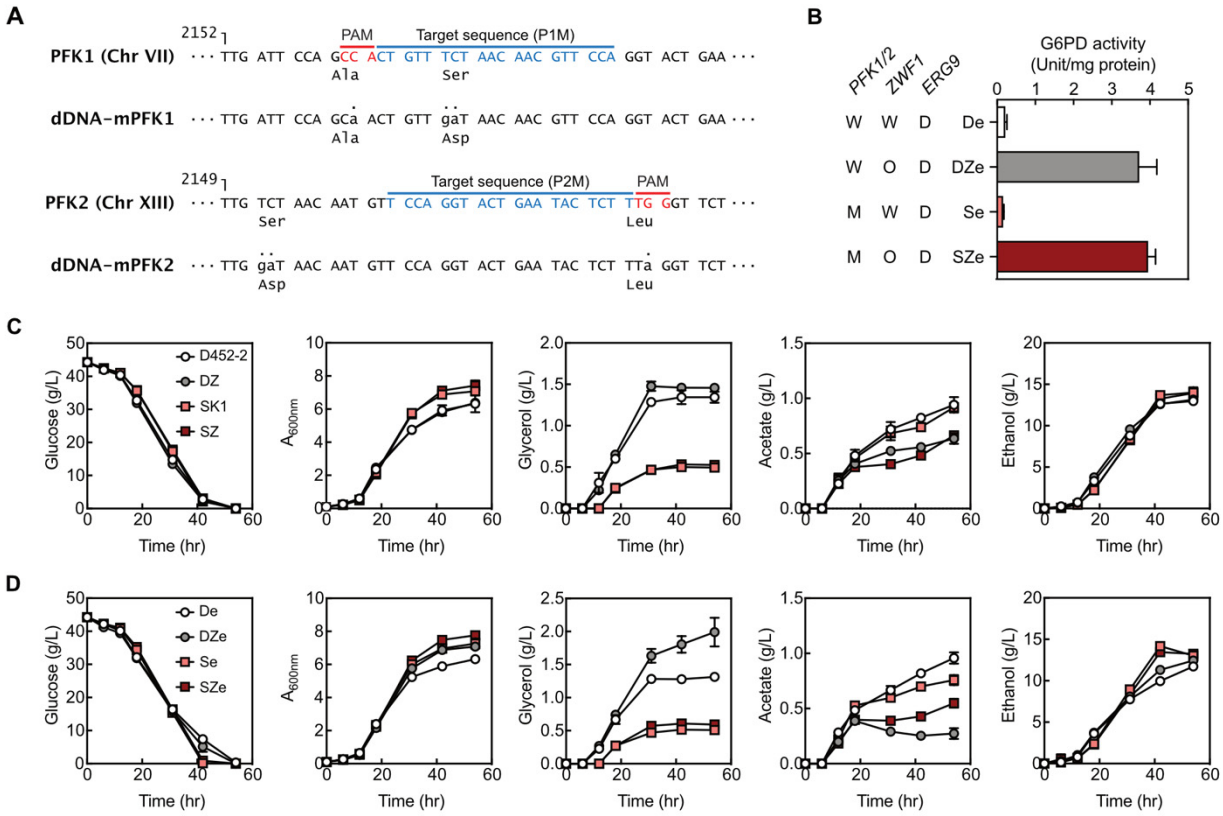
A
PFK1 (Chr VII)
dDNA-mPFK1
PFK2 (Chr XIII)
dDNA-mPFK2
PAM
Target sequence (P1M)
Target sequence (P2M)
B
PFK1/2
ZWF1
ERG9
G6PD activity
(Unit/mg protein)
De
DZe
Se
SZe
C
D
D452-2
DZ
SK1
SZ
Glucose (g/L)
A600nm
Glycerol (g/L)
Acetate (g/L)
Ethanol (g/L)
Time (hr)

Fig. 3.

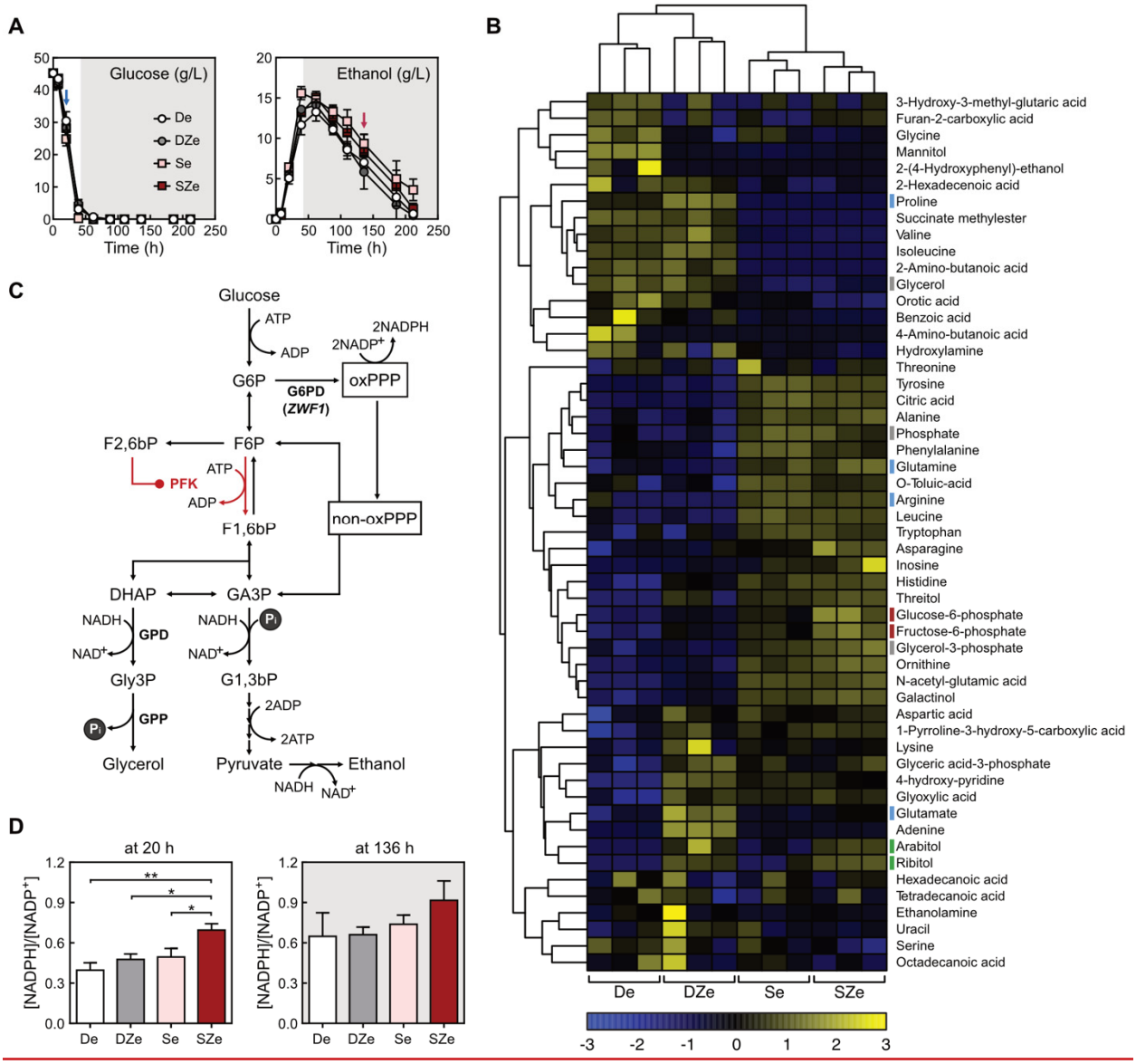
A
Glucose (g/L)
Ethanol (g/L)
De
DZe
Se
SZe
Time (h)
B
3-Hydroxy-3-methyl-glutaric acid
Furan-2-carboxylic acid
Glycine
Mannitol
2-(4-Hydroxyphenyl)-ethanol
2-Hexadecenoic acid
Proline
Succinate methylester
Valine
Isoleucine
2-Amino-butanoic acid
Glycerol
Orotic acid
Benzoic acid
4-Amino-butanoic acid
Hydroxylamine
Threonine
Tyrosine
Citric acid
Alanine
Phosphate
Phenylalanine
Glutamine
O-Toluic-acid
Arginine
Leucine
Tryptophan
Asparagine
Inosine
Histidine
Threitol
Glucose-6-phosphate
Fructose-6-phosphate
Glycerol-3-phosphate
Ornithine
N-acetyl-glutamic acid
Galactinol
Aspartic acid
1-Pyrroline-3-hydroxy-5-carboxylic acid
Lysine
Glyceric acid-3-phosphate
4-hydroxy-pyridine
Glyoxylic acid
Glutamate
Adenine
Arabitol
Ribitol
Hexadecanoic acid
Tetradecanoic acid
Ethanolamine
Uracil
Serine
Octadecanoic acid
De
DZe
Se
SZe
C
Glucose
ATP
ADP
2NADPH
2NADP+
G6P
G6PD
(ZWF1)
oxPPP
F2,6bP
F6P
PFK
ATP
ADP
F1,6bP
non-oxPPP
DHAP
GA3P
NADH
NAD+
GPD
Gly3P
G1,3bP
GPP
2ADP
2ATP
Glycerol
Pyruvate
Ethanol
D
at 20 h
at 136 h
[NADPH]/[NADP+]
De
DZe
Se
SZe

Fig. 4.

A

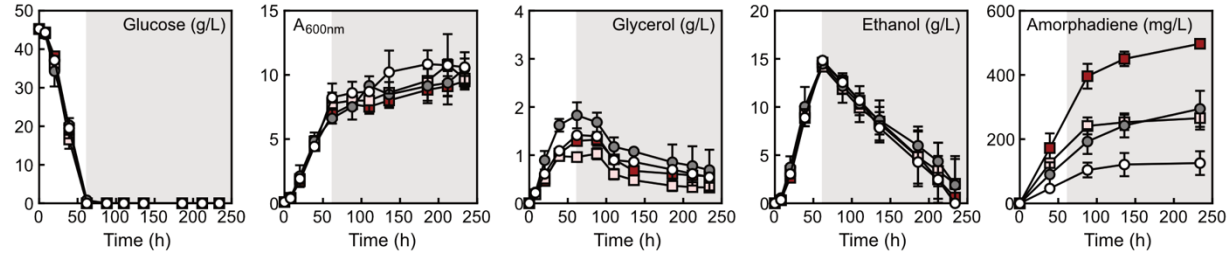

B

	ZWF1	*PFK1/2*	*ERG9*	Amorphadiene yield (mg/g)	
				Glucose phase	Ethanol phase
○ De-EHA	W	W	D	1.83 ± 0.22	1.73 ± 1.15
● DZe-EHA	O	W	D	3.62 ± 1.47	10.27 ± 3.54
□ Se-EHA	W	M	D	4.39 ± 0.42	2.44 ± 0.59
■ SZe-EHA	O	M	D	6.72 ± 1.78	8.39 ± 3.65

Supporting Information for:

"Redirection of the glycolytic flux enhances isoprenoid production in *Saccharomyces cerevisiae*"

Suryang Kwak[1,2], Eun Ju Yun[2,3], Stephan Lane[1,2], Eun Joong Oh[1,2], Kyoung Heon Kim[3], and Yong-Su Jin[1,2]*

[1]Department of Food Science and Human Nutrition, University of Illinois at Urbana-Champaign, Urbana, IL, USA

[2]Carl R. Woese Institute for Genomic Biology, University of Illinois at Urbana-Champaign, Urbana, IL, USA

[3]Department of Biotechnology, Korea University, Seoul, Republic of Korea

*Corresponding author information:

Dr. Yong-Su Jin

1206 West Gregory Dr., Urbana, Illinois, 61801

Email: ysjin@illinois.edu, phone: 217-333-7981

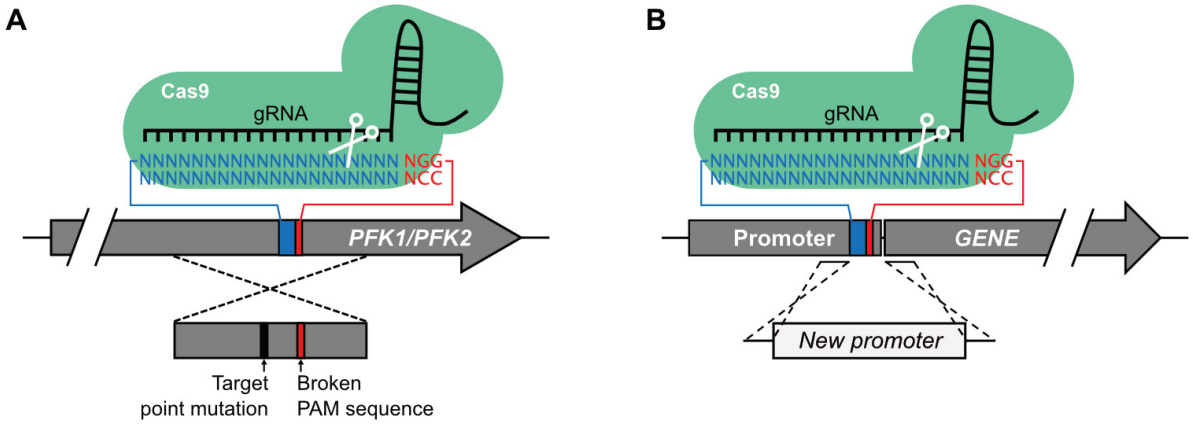

Fig. S1. Schematics of mutagenesis (A) and promoter substitution (B) using CRISPR-Cas9 genome editing in this study.

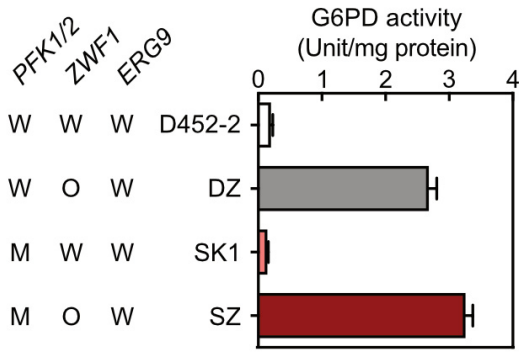

Fig. S2. Glucose-6-phosphate dehydrogenase (G6PD) activities of wild-type and engineered yeast strains before down-regulation of *ERG9*. Activity assays were conducted in quadruplicate independently, and the error bars denote the standard deviation from the means. W denotes wild-type, O denotes overexpression, and M denotes mutation of the corresponding gene.

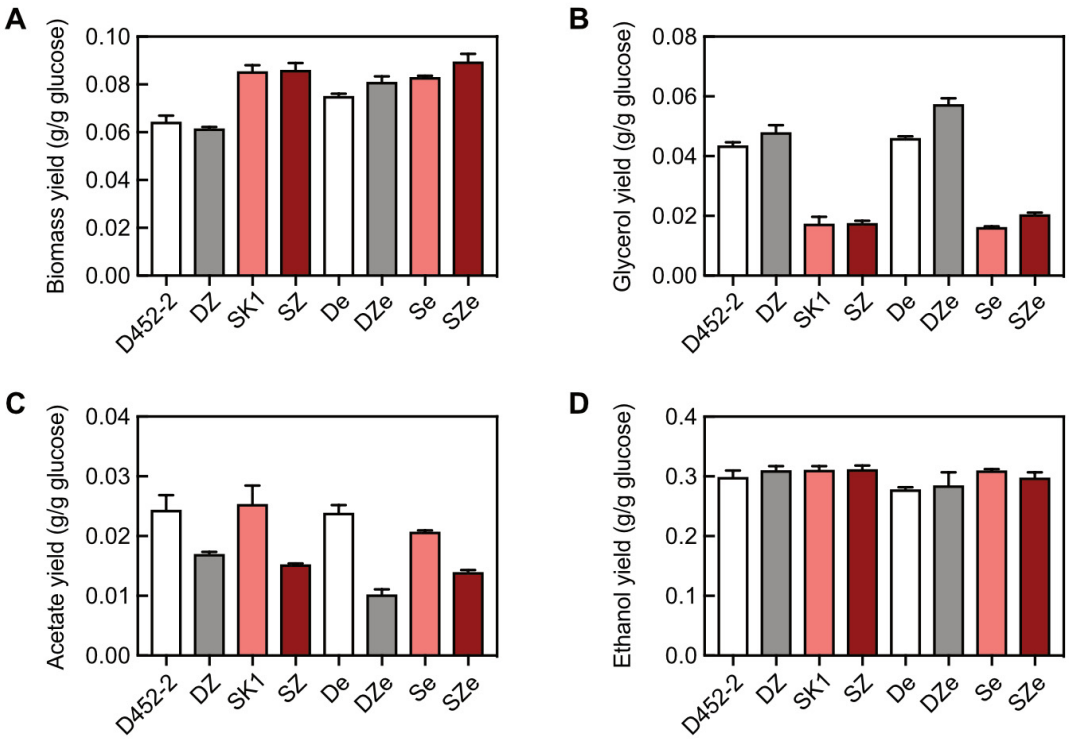

Fig. S3. Comparison of biomass (A), glycerol (B), acetate (C), and ethanol yields (D) of engineered yeast strains grown on glucose. The error bars of culture profiles denote the standard deviation of two independent experiments (Fig. 2c and 2d).

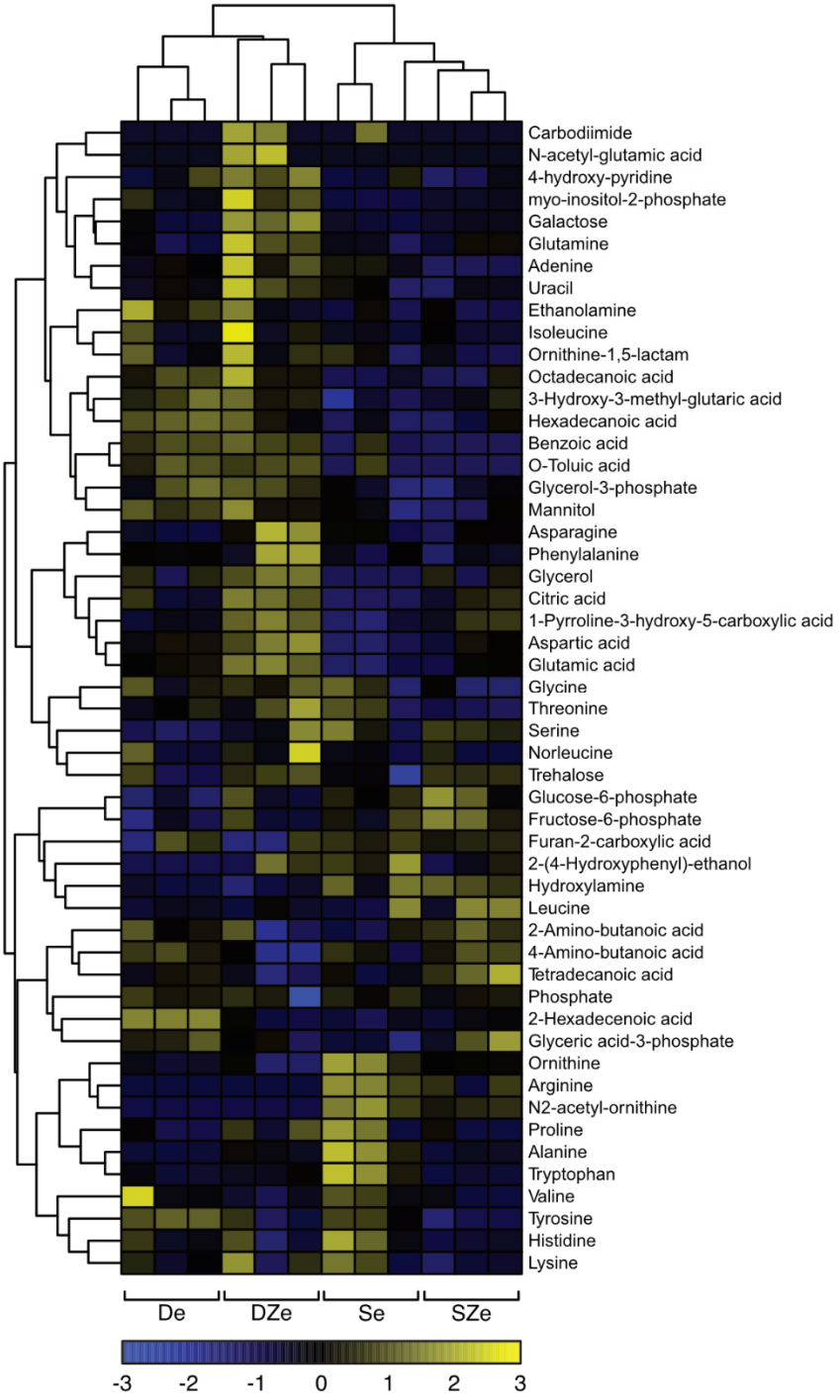

Fig. S4. A heat map and hierarchical cluster analysis (HCA) of 52 intracellular metabolites of engineered strains during ethanol utilization.

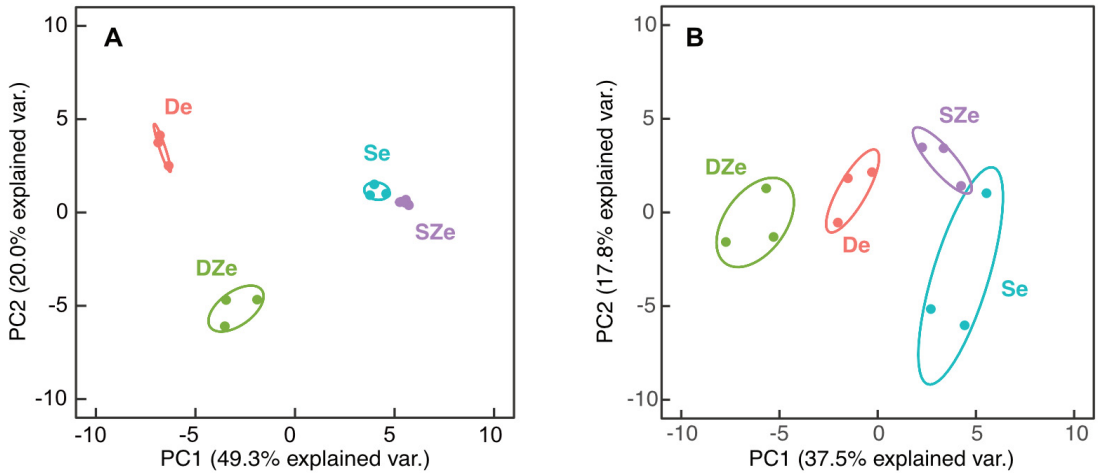

Fig. S5. Principal component analysis (PCA) scatter plots generated from the 53 intracellular metabolites of engineered strains on glucose (A) and ethanol (B).

Table S1. Plasmids used in this study.

Name	Description	Reference
Cas9-NAT	Cas9 expression plasmid with *NAT1* marker	[1]
pRS42K	2μ origin, *KanMX*	EUROSCARF
pRS42H	2μ origin, *hph*	EUROSCARF
pRS42K-P1M	pRS42K, gRNA cassette targeting the mutation site of *PFK1*	This study
pRS42H-P2M	pRS42H, gRNA cassette targeting the mutation site of *PFK2*	This study
pRS42K-PZ	pRS42K, gRNA cassette targeting promoter region of *ZWF1*	This study
pRS42H-PE	pRS42H, gRNA cassette targeting promoter region of *ERG9*	This study
pRS423	2μ origin, *HIS3*	[2]
pRS425	2μ origin, *LEU2*	[2]
pRS426	2μ origin, *URA3*	[2]
pRS423-ERG10	pRS423, P_{TDH3}-*ERG10*-T_{CYC1}	[3]
pRS425-tHMG1	pRS425, P_{TDH3}-*tHMG1*-T_{CYC1}	[4]
pRS426-ADS	pRS426, P_{CCW12}-*ADS*-T_{CYC1}	[4]

Table S2. Primers used in this study. Restriction sites are underlined. Target sequence regions of gRNA cassettes in fast cloning primers (FC) were bracketed. Homologous sequences for dDNA integration are lowercased. Point mutation sites were Italicized and underlined.

Name	Direction	Sequence
gRNA-f	Sense	CCCGAGCTCTCTTTGAAAAGATAATGTATGATTATG
gRNA-r	Antisense	AACTGCAGGGATCCAGACATAAAAAACAAAAAAAGCAC
FC-PZ-d	Sense	[ATAGAATAGAAAACCACATA]GTTTTAGAGCTAGAAATAGCAAG
FC-PZ-u	Antisense	[TATGTGGTTTTCTATTCTAT]CGATCATTTATCTTTCACTGCGGA
FC-PE-d	Sense	[GAAAAGACGAAGAGCAGAAG]GTTTTAGAGCTAGAAATAGCAAG
FC-PE-u	Antisense	[CTTCTGCTCTTCGTCTTTTC]CGATCATTTATCTTTCACTGCGGA
dD-mPFK1-f	Sense	gaacccaacacccaatctttaacattccaatgtgtttgattccagc*a*actgtt*gat*aaca
dD-mPFK1-r	Antisense	caggtatcaacaccaagtgagtattcagtacctggaacgttgtt*atc*aacagt*t*gctgga
dD-mPFK2-f	Sense	agctttcagaatcccaatggtcttgataccagctactttg*gat*aacaatgttccaggtactgaatactct
dD-mPFK2-r	Antisense	acaacatcacagtattccattagagcattcaaagcggtatcagaacc*t*aaagagtattcagtacctggaa
dD-PZC-f	Sense	tccccttcccctctccaattggctgtatagacagaaagagtaaatcca CCACCCATGAACCACAC
dD-PZC-r	Antisense	aagacagatatgacggtatttttttcgaatttgacggggccttcactcat TATTGATATAGTGTTTAAGCGAATG
dD-PES-f	Sense	agttaggacaggggcaaagaataagagcacagaagaaga ATTTGCGCTGGTTTTTTAT
dD-PES-r	Antisense	tcgaccggatgcaatgccaattgtaatagctttcccat CACTTACTGCCACTGCCA
Conf-PFK1-f	Sense	GCCAGTATCTGACAGACTAAACAT
Conf-PFK1-r	Antisense	GCTCATTGTTATGTGTATCATATCG
Conf-PFK2-f	Sense	CCATTGTTAATGTCGGTGCT
Conf-PFK2-r	Antisense	GATAATATTGGTTTCATGGGGTAG
Conf-PZ-f	Sense	TTTGGCTCAAGGTGTGG
Conf-PZ-r	Antisense	CCATCTTGAAGAACTGTTCG
Conf-PE-f	Sense	TCTGTTCTTTCGTCCCG
Conf-PE-f	Antisense	CCGATGATAGATTTGCCC

Table S3. Target sequences of gRNA used for CRISPR-Cas9 genome editing in this study.

Name	Sequence	Description
P1M	TGGAACGTTGTTAGAAACAG	Near the 2172nd base pair of *PFK1*, Chr VII
P2M	TCCAGGTACTGAATACTCTT	Near the 2154th base pair of *PFK2*, Chr XIII
PZ	ATAGAATAGAAAACCACATA	Promoter region of *ZWF1*, Chr XIV
PE	GAAAAGACGAAGAGCAGAAG	Promoter region of *ERG9*, Chr VIII

Table S4. Comparison of performances of representative amorphadiene-producing engineered *S. cerevisiae.*

Name	Strain descriptions	Medium	Amorphadiene production (time point)	Reference
EPY224	BY4742 pRS425-P_{GAL1}-ADS P_{GAL1}-tHMGR P_{GAL1}-upc2-1 erg9::P_{MET3}-ERG9 P_{GAL1}-tHMGR P_{GAL1}-ERG20	Defined medium with galactose	153 mg/L (144 h)	[5]
PDB108	EPY224 pESC-P_{GAL1}-ALD6-P_{GAL10}-SEacs^{L641P}	Defined medium with galactose	123 mg/L (192 h)	[6]
EPY213	BY4742 pRS425-P_{GAL1}-ADS erg9::P_{MET3}-ERG9 P_{GAL1}-tHMGR P_{GAL1}-upc2-1	Defined medium with galactose and glucose	ca. 125 mg/L/OD (120 h)	[7]
EPY230	BY4742 pRS425(Leu2d)-P_{GAL1}-ADS P_{GAL1}-tHMGR P_{GAL1}-upc2-1 erg9::P_{MET3}-ERG9 P_{GAL1}-tHMGR P_{GAL1}-ERG20	Defined medium with galactose and glucose	ca. 100 mg/L (144 h)	[8]
		YP medium with galactose and glucose	ca. 800 mg/L (144 h)	[8]
M246	BDXe δ::PCUP1–tHMG, δ::PCUP1–mtFDPS, δ::PCUP1–mtADS	Defined medium with glucose	ca. 20 mg/L (120 h)	[9]
Y337	CEN.PK2 erg9Δ::kanr P_{MET3}-ERG9, leu2-3,112::HIS P_{GAL1}-MVD1 P_{GAL10}-ERG8 his3Δ1::HIS P_{GAL1}-ERG12 P_{GAL10}-ERG10ade1Δ::P_{GAL1}-tHMG1 P_{GAL10}-IDI1 ADE1 ura3-52::P_{GAL1}-tHMG1 P_{GAL10}-ERG13 URA3trp1-289::P_{GAL1}-tHMG1 P_{GAL10}-ERG20 TRP1 pAM426 (P_{GAL1}-ADS) gal1Δ gal7Δ gal10Δ::HphA	Defined medium with glucose (initial carbon source), ethanol (fed-batch), and galactose (inducer only)	41 g/L (116 h)	[10]
YCF-005	MTCC 3157 erg9::pMET3-ERG9 pY01FPPS-ADS (fusion)	Defined medium with galactose	25.06 mg/L (80 h)	[11]

M3-2nd	BY4742 pRS425-P_{GAL1}-ADS δ::P_{GAL1}–ERG10 δ::P_{GAL1}–ERG13 δ::P_{GAL1}–tHMG1 δ::P_{GAL1}–ERG12 δ::P_{GAL1}–ERG8 δ::P_{GAL1}–ERG19 δ::P_{GAL1}–IDI1 δ::P_{GAL1}–ERG20	Defined medium with galactose	64 mg/L (120 h)	[12]
M4-D1-L	BY4742 pRS415-P_{GAL1}-ADS δ::P_{GAL1}–ERG10 δ::P_{GAL1}–ERG13 δ::P_{GAL1}–tHMG1 δ::P_{GAL1}–ERG12 δ::P_{GAL1}–ERG8 δ::P_{GAL1}–ERG19 δ::P_{GAL1}–IDI1 δ::P_{GAL1}–ERG20 erg9::P_{ERG1}-ERG9	Defined medium with galactose and glucose	350 mg/L (96 h)	[13]
HX4HEA-EE	SR7 (xylose-fermenting *S. cerevisiae* D452-2) P_{TDH3}-tHMG1 P_{TDH3}-ERG10 P_{CCW12}-ADS erg9::P_{ERG1}-ERG9	Defined medium with glucose	196 mg/L (114 h)	[4]
		Defined medium with xylose	254 mg/L (114 h)	[4]
SZe-EHA	D452-2 pfk1::mtPFK1 pfk2::mtPFK2 zwf1::P_{CCW12}-ZWF1 pRS423-P_{TDH3}-ERG10 pRS425-P_{TDH3}-tHMG1 pRS426-P_{CCW12}-ADS	Defined medium with glucose	396 mg/L (88 h)	This study
			497 mg/L (234 h)	This study

Reference

[1] G. C. Zhang, I. I. Kong, H. Kim, J. J. Liu, J. H. D. Cate, Y. S. Jin, *Appl. Environ. Microbiol.* **2014**, *80*, 7694.

[2] D. Mumberg, R. Müller, M. Funk, *Gene* **1995**, *156*, 119.

[3] E. J. Yun, S. Kwak, S. R. Kim, Y. C. Park, Y. S. Jin, K. H. Kim, *J. Biotechnol.* **2015**, *209*, 23.

[4] S. Kwak, S. R. Kim, H. Xu, G. C. Zhang, S. Lane, H. Kim, Y. S. Jin, *Biotechnol. Bioeng.* **2017**, *114*, 2581.

[5] D. K. Ro, E. M. Paradise, M. Ouellet, K. J. Fisher, K. L. Newman, J. M. Ndungu, K. A. Ho, R. A. Eachus, T. S. Ham, J. Kirby, M. C. Y. Chang, S. T. Withers, Y. Shiba, R. Sarpong, J. D. Keasling, *Nature* **2006**, *440*, 940.

[6] Y. Shiba, E. M. Paradise, J. Kirby, D. K. Ro, J. D. Keasling, *Metab. Eng*. **2007**, *9*, 160.

[7] E. M. Paradise, J. Kirby, R. Chan, J. D. Keasling, *Biotechnol. Bioeng*. **2008**, *100*, 371.

[8] D. K. Ro, M. Ouellet, E. M. Paradise, H. Burd, D. Eng, C. J. Paddon, J. D. Newman, J. D. Keasling, *BMC Biotechnol*. **2008**, *8*, 83.

[9] M. Farhi, E. Marhevka, T. Masci, E. Marcos, Y. Eyal, M. Ovadis, H. Abeliovich, A. Vainstein, *Metab. Eng*. **2011**, *13*, 474.

[10] P. J. Westfall, D. J. Pitera, J. R. Lenihan, D. Eng, F. X. Woolard, R. Regentin, T. Horning, H. Tsuruta, D. J. Melis, A. Owens, S. Fickes, D. Diola, K. R. Benjamin, J. D. Keasling, M. D. Leavell, D. J. McPhee, N. S. Renninger, J. D. Newman, C. J. Paddon, *Proc. Natl. Acad. Sci. U. S. A.* **2012**, *109*, E111.

[11] R. R. Baadhe, N. K. Mekala, S. R. Parcha, Y. Prameela Devi, *J. Anal. Methods Chem*. **2013**, *2013*, 140469.

[12] J. Yuan, C. B. Ching, *Biotechnol. Bioeng*. **2014**, *111*, 608.

[13] J. Yuan, C. B. Ching, *Microb. Cell Factories* **2015**, *14*, 38.